Article ID: 1671-3664(2004)01-0039-12

Liquefaction mitigation in silty soils using composite stone columns and dynamic compaction

T. Shenthan[1†], R. Nashed[1†], S. Thevanayagam[1‡] and G. R. Martin[2§]

1. *Department of Civil Engineering, UB, USA*
2. *Department of Civil Engineering, USC, Los Angeles, CA, USA*

Abstracts: The objective of this study is to develop an analytical methodology to evaluate the effectiveness of vibro stone column (S.C.) and dynamic compaction (D.C.) techniques supplemented with wick drains to densify and mitigate liquefaction in saturated sands and non-plastic silty soils. It includes the following: (i) develop numerical models to simulate and analyze soil densification during S.C. installation and D.C. process, and (ii) identify parameters controlling post-improvement soil density in both cases, and (iii) develop design guidelines for densification of silty soils using the above techniques. An analytical procedure was developed and used to simulate soil response during S.C. and D.C. installations, and the results were compared with available case history data. Important construction design parameters and soil properties that affect the effectiveness of these techniques, and construction design choices suitable for sands and non-plastic silty soils were identified. The methodology is expected to advance the use of S.C. and D.C. in silty soils reducing the reliance on expensive field trials as a design tool. The ultimate outcome of this research will be design charts and design guidelines for using composite stone columns and composite dynamic compaction techniques in liquefaction mitigation of saturated silty soils.

Keywords: liquefaction mitigation; silty soils; composite stone columns; dynamic compaction

1 Introduction

Liquefaction is one of the primary causes of lateral spreading, failures of bridge foundations, embankments, and ports and harbor facilities during earthquakes (e.g. 1964 Alaska earthquake, 1995 Kobe earthquake). Soil densification techniques using vibro-stone column (Fig.1(a)) and deep dynamic compaction (Fig.2(a)) are proven ground improvement methods for liquefaction mitigation in loose saturated sands containing less than 15% non-plastic silts and less than 2% of clay particles (FHWA 2001, Mitchell *et al.*,1995, Andrus and Chung, 1995). Silty sands containing excessive fines have been considered difficult to densify using the above densification methods. However, recent case histories show that provision of pre-installed supplementary wick drains around the vibro-stone columns (Figs.1(b)) and impact locations (Fig.2(b)) help densification of silty soils during vibro-stone column installation or dynamic compaction (Andrews, 1998; Dise *et al.*, 1994; Luchring *et al.*, 2001).

Correspondence to: T. Shenthan, Department of Civil Engineering, University at Buffalo, NY, USA
Tel: 716 645-2114; Fax: 716 645-3733
E-mail: theva@eng.buffalo.edu
[†]Graduate Research Assistant; [‡]Associate Professor; [§]Professor

Supported by: Federal Highway Administration (FHWA) Under Grant No. DTFH61-98-C-0094
Received date: 2004-03-19; **Accepted date:** 2004-05-15

Vibro-stone column installation process involves insertion of a vibratory probe with rotating eccentric mass. The probe plunges into the ground due to its self-weight and vibratory energy, which facilitates penetration of the probe. Once the specified depth (depth of stone column) is reached, the probe is withdrawn in steps (lifts) of about 1m. During withdrawal of the probe, the hole is backfilled with gravel. During each lift the probe is then reinserted expanding the stone column diameter. This process is repeated several times until a limiting condition is achieved. No detailed analytical procedures are available to determine the densification achievable during stone column installation or the effects of various construction choices such as stone column spacing, diameter, and wick drain size and spacing on the degree of improvement. The current state of practice depends mainly on previous experience or field test programs to determine the applicability of the technique and choice of stone column spacing, etc. at a given site. Based on field data, Baez (1995) outlines an empirical approach (Fig. 8, introduced later) for design of vibro-stone columns, without wick drains, to improve sandy soils containing less than 15% silt.

The D.C. technique involves high-energy impacts to the ground surface by systematically dropping heavy weights of 6 to 35 tons from heights ranging from 12 to 40 m to compact the underlying ground using heavy crawler cranes. Based on previous field experience (Lukas, 1986, 1995), for an average cumulative applied energy in the range of 1 to 3 MJ/m^2, the maximum depth

of improvement (d_{max}) that can be achieved due to D.C. is given by:

$$d_{max} = n\,(WH)^{1/2} \tag{1}$$

where, W is the dropped weight in tonnes, and H is the height of drop in m. The value of n depends on soil type, and decreases with an increase in degree of saturation. Although Eq.(1) is a useful guide, design choices such as impact weight, height of drop, impact grid spacing, time lag between impacts, total number of passes required to achieve a specified level of relative density or SPT/CPT penetration resistance are made based on field trials. Again, no detailed analytical procedures are available to determine the densification achievable or to analyze the effects of various operational parameters on the degree of improvement.

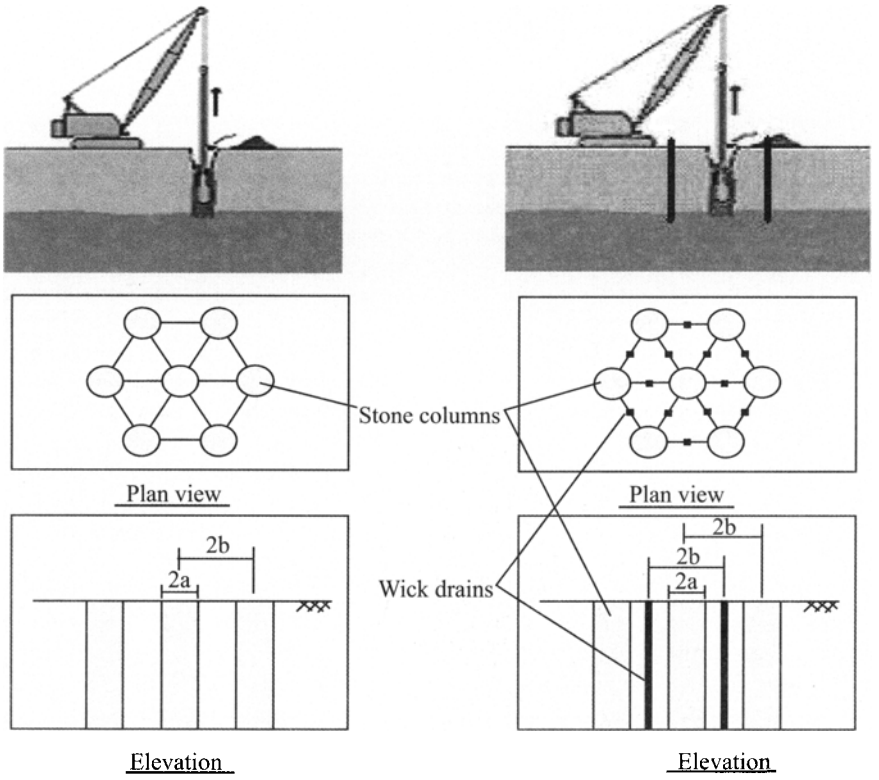

(a) Traditional vibro-stone column (b) Composite vibro-stone column

Fig. 1 Vibro-stone columns and composite vibro-stone column

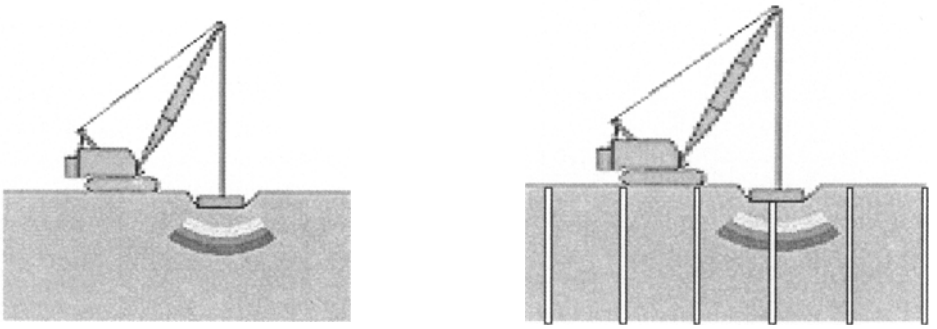

(a) Traditional dynamic compaction (b) Composite dynamic compaction

Fig. 2 Dynamic compaction

This paper presents a brief summary of recent work conducted to develop a simple analytical methodology to simulate soil response during vibro-stone column installation and dynamic compaction, quantify soil

densification during vibro-stone column installation and dynamic compaction in saturated sands and silty soils, and assess the effect of various construction/ design choices and soil parameters on the degree of improvement achievable.

2 Semi-theoretical framework

Densification of saturated sands and silty soils by vibro-stone column and dynamic compaction is essentially a process involving vibration of the soil causing excess pore pressure development, liquefaction, and consolidation of the soil leading to concurrent densification. Vibro-stone column also involves expansion of a zero cavity and associated pore pressures and densification of the soil. This paper presents a methodology to simulate pore pressure developments in the soil due to vibratory energy imparted during installation, and subsequent consolidation of the soil and densification. Simple attenuation relationships are used to estimate the energy dissipated in the soil. Experimental data based on energy principles is used to estimate the pore pressures generated as a function of the energy dissipated. Coupled consolidation equations are used to quantify densification and study the effects of various soil parameters and design/construction choices on the degree of improvement achievable.

2.1 Energy radiation and attenuation

Consider vibro-stone column (S.C.) (Fig.3) and dynamic compaction (D.C.) impact (Fig.4) processes. The energy delivered at the source by the vibratory probe and by a falling weight propagates through the surrounding soil as body waves (compressional and shear waves) in case of S.C., and body waves and surface waves (Rayleigh waves) in the case of D.C., repectively. Field observations indicate that the ground vibrations caused by S.C. is in the range of 30 to 50 Hz (FHWA, 2001) and between 2 to 20 Hz (Mayne 1985) for D.C. A solution for energy dissipated (per unit volume of soil), the associated pore water pressures, and densification at any point in the soil requires a reasonably accurate quantification of energy partitions in the above three categories and their spatial attenuation relationships. The problem is complex due to non-uniformity in stress field, stress and density dependent soil properties, and changes in the stress field, pore water pressures, and soil densities in the ground during and immediately following the energy delivery. In order to circumvent this problem, as a first order approximation, models for energy partition in elastic half-space coupled with field-observation based attenuation models are used herein.

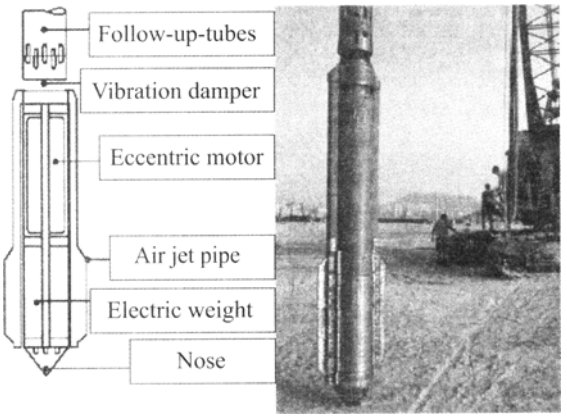

(a) Cross section through a vibroprobe

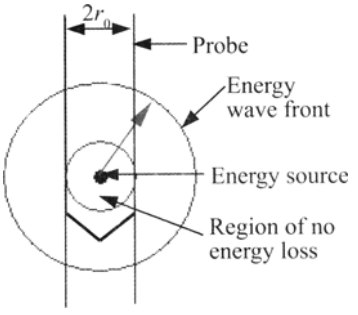

(b) Radiation of vibratory energy-schematic

Fig. 3 The vibratory probe and energy propagation

Past studies indicate that the energy partitioning in the form of shear, compressional, and Raleigh waves due to a harmonic uniform vertical stress on a flexible disk of radius r_0 acting on an elastic half-space is dependent on frequency parameter a_0 ($= \omega r_0 / c_s$, where, ω = angular frequency in Hz., and c_s = shear wave velocity in m/s) (Fig. 5(a)) and Poisson's ratio (Miller and Pursey, 1955; Meek and Wolf, 1993). Further, Richart *et al.*, (1970) show that Raleigh wave amplitude varies with dimensionless depth (depth/L_R) as shown in Fig. 5(b) where, L_R = wavelength of Rayleigh wave. Rayleigh wave amplitude ratio attenuates with depth very rapidly to about 10% at a depth of about 1.6 L_R. As a first order approximation, if the above model is used to determine the energy partitioning for D.C, the frequency parameter a_0 tends to be less than 1 for typical values of r_0 corresponding to impact weights used in dynamic compaction, c_s of soils, and frequencies in the range of 2 to 20 Hz, and hence Rayleigh waves account for about two thirds of impact energy transfer and body waves account for the remaining one third. For D.C, further, considering radiation damping, the energy content of

body wave is assumed to be uniformly distributed on a hemispherical surface of the wave front, while energy content of Rayleigh wave is assumed to be spreading radially along a cylindrical surface, and is also assumed to attenuate with depth as shown in Fig.5(b) for Poisson's ratio ν =0.25.

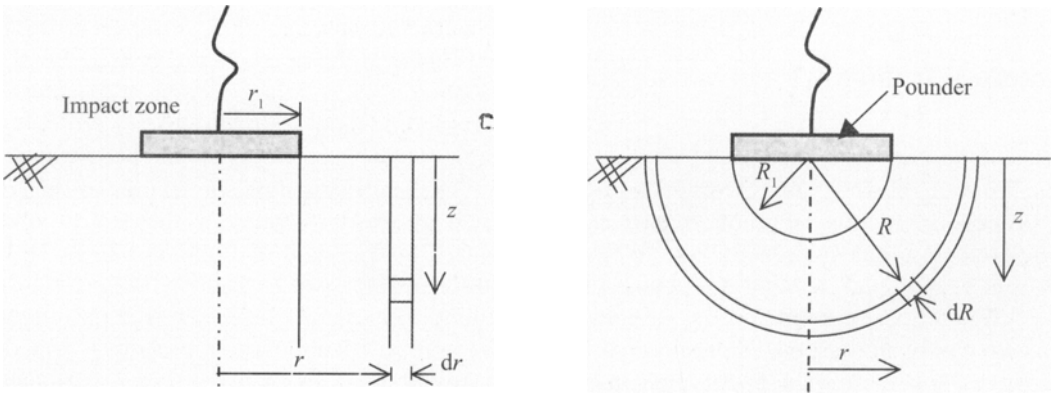

Fig. 4 Energy partitioning – dynamic compaction

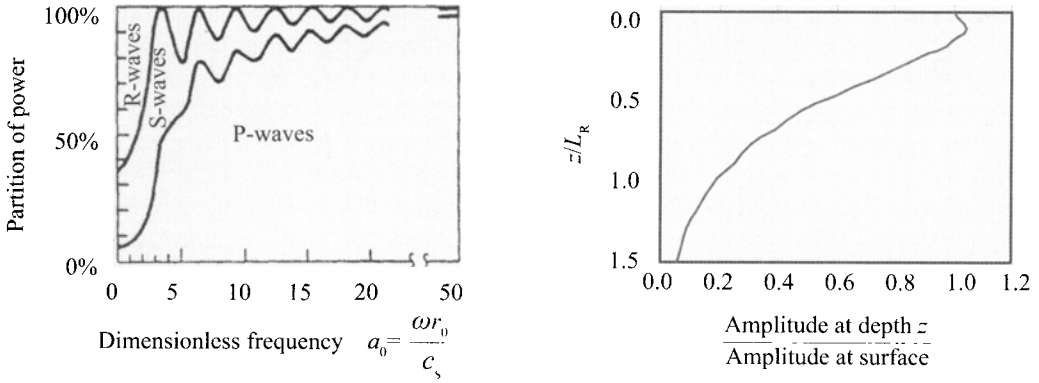

(a) Partition of energy – surface load (b) Wave amplitude (Rayleigh wave)

Fig. 5 Partition of energy and wave amplitude

Material damping occurs as a result of energy loss due to hysteresis damping and internal sliding of soil particles. The energy loss depends on frequency of loading, soil type, stress conditions, and strain level. Field observations indicate surface wave attenuation due to material damping is given by (Dowding, 1996):

$$a = a_1 e^{-\alpha(r-r_1)} \tag{2}$$

where, a_1 = amplitude of vibration at distance r_1 from the source, a = amplitude of vibration at distance r, and α = attenuation coefficient due to material damping. Energy attenuation is related to the square of the amplitude of vibration; the corresponding energy attenuation relationship is given by

$$E = E_1 e^{-2\alpha(r-r_1)} \tag{3}$$

where, E_1 = energy content at a distance r_1 from the source, E = energy content at a distance r.

Based on the above considerations, the energy loss per unit volume of soil due to Rayleigh waves w_R and body waves w_B, respectively, in the case of D.C., are given by

$$w_R(r,z) = F(0.67WH)\frac{\alpha e^{-2\alpha r}}{\pi r} \tag{4}$$

$$F = \frac{f^2(\frac{z}{L_R})}{\int_0^\infty f^2(\frac{z}{L_R})dz} \tag{5}$$

$$w_B(r,z) = (0.33WH)\frac{\alpha e^{-2\alpha R}}{\pi R^2} \tag{6}$$

where, $R = \sqrt{(r^2+z^2)}$, f = amplitude ratio given by Fig.5(b), and r and z are radial and vertical coordinates, respectively.

In the case of S.C., assuming that radiation damping is due to body waves spreading along a spherical wave front and it is uniformly distributed on a spherical surface of the wave front, the energy loss per unit time per unit volume of soil takes the form:

$$w = W_0 \frac{\alpha e^{-2\alpha(r-r_0)}}{2\pi r^2} \tag{7}$$

where, $W_0 = \eta_0 P_0$, P_0= power rating of the vibratory probe, η_0 = probe efficiency. As excess pore pressure develops due to vibration during S.C process, the soil becomes weak. Since the amplitude of vibration of the probe is limited (FHWA, 2001), the energy imparted to the surrounding soil would decrease resulting in a reduced efficiency. When the pore pressures dissipate, and the soil is sufficiently densified, the energy transfer rate would increase. In this paper, this phenomenon was taken into account considering the energy transfer rate to decay with increasing excess pore pressure:

$$w = W_0 \frac{\alpha e^{-2\alpha(r-r_0)}}{2\pi r^2} e^{-\beta(r_u)_{av}} \tag{8}$$

where $(r_u)_{av}$=the average excess pore pressure ratio within the soil surrounding the probe up to an effective radial distance r_e, and β=a constant. A detailed discussion on the applicability and limitations of the above attenuation relationships, and ongoing further work on attenuation relationships are reported in Shenthan (2004), and Nashed (2004).

2.2 Pore pressure generation

Based on a large experimental database and theoretical considerations, excess pore water pressure generated due to undrained cyclic loading has been related to frictional energy loss in the soil by Thevanayagam *et al.* (2002) as:

$$r_u = 0.5 \log_{10}\left(100 \frac{w_c}{w_L}\right), \quad \frac{w_c}{w_L} > 0.05 \tag{9}$$

where, r_u=excess pore pressure ratio (u/σ_0'), σ_0'=initial mean effective confining pressure, w_c = cumulative energy loss per unit volume of soil, and w_L = energy per unit volume required to cause liquefaction.

In the case of S.C. process, in addition to vibration-induced excess pore pressure, a significant amount of pore pressure is generated due to cavity expansion as well. Initial insertion of the probe into the ground can be considered as expanding a zero cavity to a diameter the same as that of the probe. Filling of this cavity by stones and inserting the probe further expands the cavity by pushing the stone backfill radially outwards. Lifting the probe causes slight contraction of the cavity. Repeated lifting, filling, and insertion of the probe cause repeated cavity expansions. Shenthan *et al.* (2004) outline a simplified approach to estimate excess pore pressures induced during such cavity expansions and contractions.

2.3 Pore pressure dissipation and densification

The governing equation for pore pressure dissipation in the soil is:

$$\frac{\partial u}{\partial t} = \frac{k_h}{\gamma_w m_v}\left(\frac{\partial^2 u}{\partial r^2} + \frac{1}{r}\frac{\partial u}{\partial r} + \frac{1}{r^2}\frac{\partial^2 u}{\partial \theta^2}\right) + \frac{k_v}{\gamma_w m_v}\frac{\partial^2 u}{\partial z^2} + \frac{\partial u_g}{\partial t} \tag{10}$$

where k_h and k_v are hydraulic conductivity of the soil in horizontal and vertical directions, respectively; m_v=volume compressibility of the soil; u = excess pore water pressure at coordinates (r, θ, z); u_g = excess pore pressure generated due to vibration and cavity expansion (in the case of S.C.); t = time; γ_w = unit weight of water; r, θ, and z are radial, angular, and vertical coordinates, respectively. In case of vibro-stone column, the term u_g stands for time dependent pore pressure generation as in the case due to vibratory energy during S.C. installation. In case of cavity expansion/contraction and D.C., excess pore pressures are assumed to be induced instantaneously.

Volumetric densification of a soil element due to excess pore pressure dissipation may be obtained by:

$$\varepsilon_v = \int m_v d\sigma' \tag{11}$$

where, ε_v=volumetric strain, and σ'=mean effective confining pressure. Seed *et al.* (1975) suggest that m_v values for sands increase from its initial value according to the following relationship, and do not decrease from the highest value obtained:

$$\frac{m_v}{m_{v0}} = \frac{\exp(y)}{1 + y + y^2/2} \geq 1,$$

$$y = a r_u^b, \quad a = 5(1.5 - D_r), \quad b = 3(4)^{-D_r} \tag{12}$$

where, m_v and D_r are initial volume compressibility and relative density of soils, respectively. For silty sands, the above equation is modified to use $(D_{rc})_{eq}$ instead of D_r to take into account the effects of fines on volume compressibility (Shenthan, 2004). Typical values for m_{v0} are adopted from Thevanayagam and Martin (2001).

3 Simulations and field comparisons

3.1 Vibro-stone column

Two sets of numerical simulations were conducted to study densification process of soils during stone column installation. In the first set of simulations, the effect of cavity expansion was neglected and the effect of vibration induced pore pressure generation and dissipation was considered. Based on experimental data available, hydraulic conductivity k was obtained as a function of silt content. In the second set of simulations, the effect of cavity expansion was included and the vibration induced pore pressures were neglected. In both set of simulations vertical dissipation was neglected in order to reduce the computational time. These simulations are presented below.

3.1.1 Energy dissipation and densification

The simulations presented herein consider soil densification due to dissipation of vibration induced pore pressures only. Figure 6 shows a composite vibro-stone column layout. The radii of the stone columns and wick drains are a and r_w, respectively. The spacing between stone columns is $2b$. The spacing between wick drains is b. The wick drains are installed first, and the surrounding stone-columns are installed next followed by installation of the center column. The numerical simulation presented in the following sections pertains to densification of the soil during installation of the center column. Using the semi-theoretical background introduced earlier, a finite-difference numerical scheme was developed to simulate this densification process in the soil surrounding the center column. Boundaries of symmetry allow reducing the computational time by requiring calculations to be done for only the representative area shown in Fig.6.

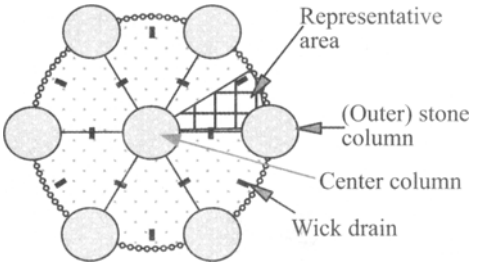

Fig. 6 Composite stone column layout

(1) Vibro-stone columns without wicks

The simulations herein consider installation of vibro-stone columns in clean sand with no wick drains (Fig. 1(a)). Three different initial densities were used: (a) D_r=40%, (b) D_r=48%, and (c) D_r=59%. Three different area replacement ratios (A_r=5.6, 10.0, and 22.5%) were assumed for each initial density, where $A_r=(A_c/A_e)\times100\%$, A_c is area of the stone-column, A_e is the tributary area ($=\pi\times D_e^2/4$), and D_e=equivalent diameter of the tributary area=1.05 times the center-to-center spacing between stone columns installed in a triangular pattern. These A_r values correspond to center-to-center stone column spacing of 4 diameters, 3 diameters, and 2 diameters, respectively. The hydraulic conductivity was assumed to be 5×10^{-6} m/s. Table 1 summarizes the probe characteristics used for the simulation. Table 2 summarizes simulation parameters. The post-improvement densification results are shown in Fig.7(a).

Table 1 Vibratory probe specifications

Length (m)	Frequency(Hz)	Power rating P_0 (kW)	η_0(%)	β	Avg. penetration rate (cm/s)
3	50	120	50	4	3

Table 2 Simulation parameters - stone column

Column dia. (m)	Column spacing (m)			k (m/s)
	A_r=5.6%	A_r=10.0%	A_r=22.5%	
0.9	3.6	2.7	1.8	5×10^{-6}

Note: Initial effective confining pressure at the depth considered is about 100 kPa.

The area replacement ratio has a significant influence on post-improvement density. This influence diminishes as the initial density increases. Although not shown in this paper, it was also found that hydraulic conductivity plays an important role and higher hydraulic conductivity leads to higher densification for the same vibratory duration (Shenthan, 2004; Thevanayagam *et al.*, 2001).

For qualitative comparison purposes, the data in Fig.7(a) may be converted to equivalent SPT blow counts $(N_1)_{60,c\text{-}s}$ using Tokimatsu and Seed (1984) relationship for clean sands, as shown in Fig.7(b). This can be compared with the field-case history database for pre- and post-improvement SPT blow counts compiled by Baez (1995) shown in Fig.8. The regression curves for post-improvement SPT blow counts obtained by Baez (1995) were based on an analysis of a number of case histories, where vibro-stone columns were used to improve sandy soil sites with less than 15% silts.

Although direct comparisons are not possible, due to lack of site-specific data, the trend found in Fig.7(b) agrees well with the trend in Fig.8. Further work is underway to verify simulation results with field trials.

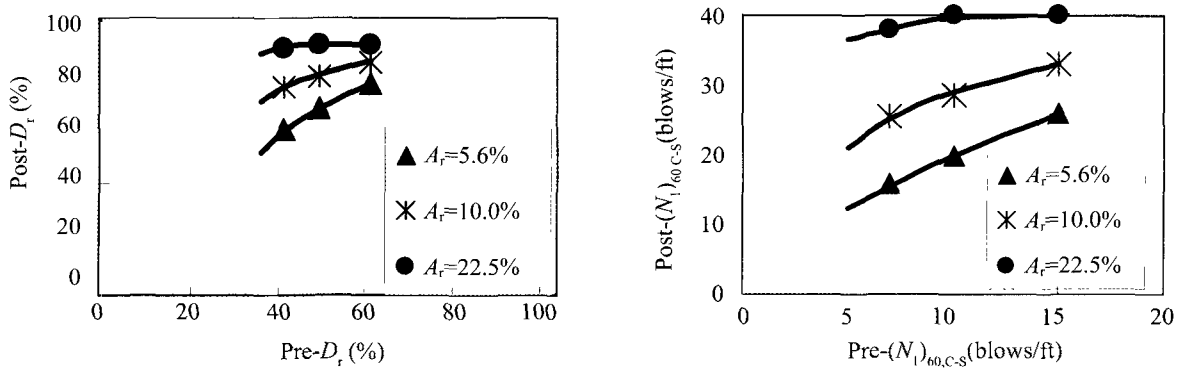

(a) Post-improvement densification result (b) Equivalent SPT blow counts $(N_1)_{60,C-S}$

Fig. 7 Vibro-stone column simulation results

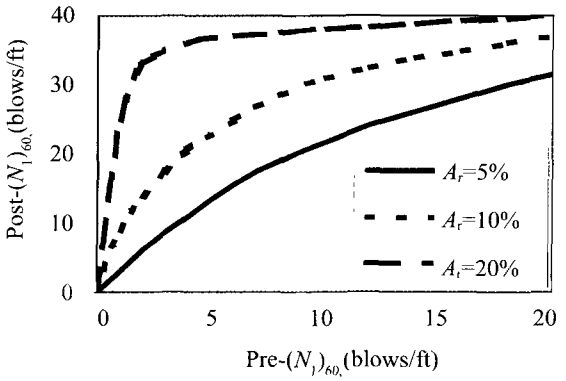

Fig. 8 Regression design curves (Baez, 1995)

(2) Composite vibro-stone column

A number of simulations were conducted to assess the effects of silt content, and area replacement ratio A_r on post improvement density of silty soils supplemented by wick drains (Fig.1(b)). Three different initial equivalent relative densities ($(D_r)_{eq}$=40, 48 and 59%, Shenthan 2004) were considered. Silt content dependent soil input parameters m_v, k, E_L were obtained from an experimental database for silty soils (Shenthan 2001, and Thevanayagam *et al.* 2001). For direct comparison purposes, the same simulations were repeated for stone columns in the same soil without wick drains (Fig.1(a)). Figs. 9(a)-(b) show the simulation results for post-improvement relative densities for A_r=10, and 22.5%, respectively, for the three different initial relative densities $(D_r)_{eq}$ considered. Without wick drains, no significant improvement is achieved for soils with hydraulic conductivity less than about 10^{-6} m/s. Although not shown in this paper, at low A_r, wick drains do not contribute to any further increase in post-improvement density for all initial densities (Shenthan *et al.*, 2004). In this case, the spacing of stone columns

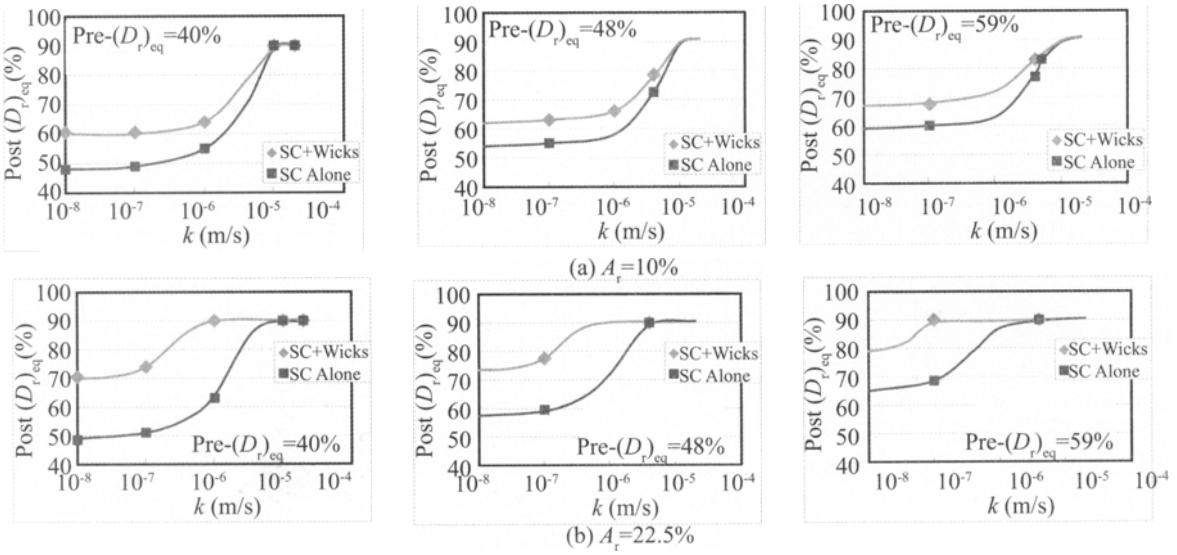

Fig. 9 Composite vibro-stone columns – simulation results

(SC=Vibro-stone column without wicks, SC + Wicks=Composite vibro-stone column)

and wick drains is too large and wick drains are far from the stone columns to be effective in reliving the pore pressures during installation and to facilitate repeated cycles of densification. As the area replacement ratio increases, influence of wick drains increases. At high area replacement ratio of about 20% or above (Fig. 9b), wick drains significantly contribute to the drainage and repeated densification of silty soils with hydraulic conductivity as low as 10^{-8}m/s. However, the degree of improvement is dependent on hydraulic conductivity.

3.1.2 Cavity expansion and densification

The simulations presented herein consider soil densification due to dissipation of cavity expansion induced pore pressures only. These simulations involved two cases, (i) stone columns with wick drains, and (ii) without wick drains. The initial density of soils was $(D_r)_{eq}$=40%. Three different area replacement ratios (A_r=10%, 15%, and 25%) were considered. Probe characteristics used for the simulation are the same as those summarized in the Table 1. Table 3 summarizes simulation parameters relevant to this analysis. Vibratory probe diameter is 0.36 m. In lifts of 1m, the probe is reinserted 7 times to build a stone column of 0.95m diameter at any given depth. Field observations indicate that this process takes about 4 to 5 minutes per lift of 1m.

The post-improvement densification results are shown in Figs.10(a), (b), and (c) for A_r=10%, 15%, and 25%, respectively. Without wick drains, highest improvement is achieved for highly permeable soils at or above 10^{-5}m/s. The post-improvement density depends on hydraulic conductivity and area replacement ratio. Addition of wick drains does not significantly affect the degree of improvement. It appears that the cavity expansion induced pore pressures do not extend far enough from the stone column and hence wick drains do not significantly contribute to drainage in this case, except for large A_r (Fig.10(c)).

Table 3 Simulation parameters - cavity expansion

Column diameter (m)	Column depth (m)	Column spacing (m)			Depth simulated (m)
		A_r=10%	A_r=15%	A_r=25%	
0.95	15	2.85	2.3	1.8	12

Note: Initial effective confining pressure at the depth considered is about 100 kPa.

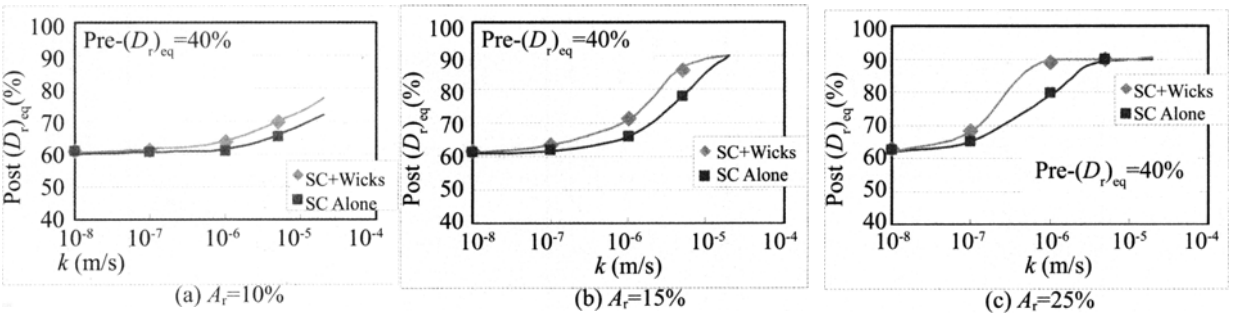

Fig. 10 Post-improvement densification - due to pore pressures induced by cavity expansion

The above results shown in Figs. 9 and 10 indicate that both cavity expansion process and ground vibration contribute to densification. Post-improvement densities due to the coupled effect of both cavity expansion and vibratory energy should be higher than those obtained by considering cavity expansion only. Further work is underway to couple these two phenomena.

3.2 Dynamic compaction

3.2.1 Comparison with case histories

The above model given by Eqs.(2)-(6) and (9)-(12) was used to simulate soil response during dynamic compaction process and quantify soil densification in sands and silty soils. First D.C. process, two case history sites were analyzed: (a) Kampung Pakar site, Malaysia (Chow *et al.*, 1992), and (b) Steinaker dam modification project (Dise *et al.*, 1994) and the results were compared with field measurements. This was followed by a parametric study.

(1) Kampung Pakar site, Malaysia

Kampung Pakar site is a development site consisting of 14 m of relatively uniform and homogeneous loose sand, with water table at about 3 m below the surface. The dynamic compaction program involved two high-energy passes carried out on 6m×6m grid pattern using a 1.83 meter square pounder weighing 15 tonnes. The design parameters are summarized in Table 4. The post-improvement simulation results are compared with the field density measurements, deduced from CPT data, in Fig. 11. The profile corresponds to the center in the six-meter square grid pattern. Considering the approximate, first-order nature of the numerical simulations, the simulation results agree reasonably well with the

measured data.

(2) Steinaker Dam modification project, Utah

In this case, the soil profile data and compaction parameters were obtained from Hayward Baker, Inc., and is reported by Nashed (2004). Briefly, the treated sandy silt contains an average fines content of 45%. Wick drains were installed on 1.5m centers to a depth of 9m and a 1.5m thick compaction pad was constructed. Perimeter well points were installed to lower the water table at least 3.7 m below the top of the compaction pad. The dynamic compaction program involved three high-energy passes (Table 4). The impact grid pattern is shown in Fig. 13. Because of the expected buildup of excess pore pressures, the drop sequence was tightly controlled. The primary pass was completed before drops were allowed at secondary locations. Similarly, for the secondary and tertiary passes. Measured data consisted of pre and post-improvement SPT profiles. Fig. 12 shows the pre and post-improvement SPT field data along with the equivalent SPT profiles obtained based on density profile results from numerical simulations (Nashed, 2004). The simulation results follow the trend observed in the field.

Table 4. Impact parameters – dynamic compaction

Parameters	Kampung Paker site, Malaysia		Steinaker Dam modification project, Utah			
	1st pass	2nd pass	Initial ironing	1st pass	2nd pass	3rd pass
Pounder weight (tonne)	15.0	15.0	30.0	30.0	30.0	30.0
Drop height (m)	20.0	25.0	18.0	30.0	30.0	30.0
No. of impacts at each grid point	10	6	2	30	30	20

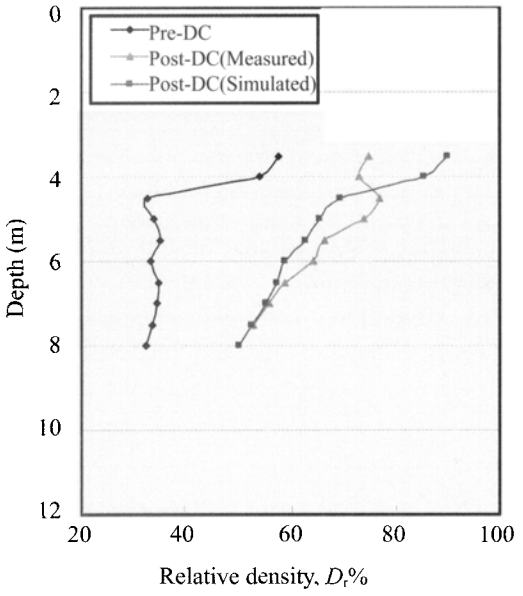

Fig. 11 Pre- and post-D.C. relative density (Kampung Pakar site, Malaysia)

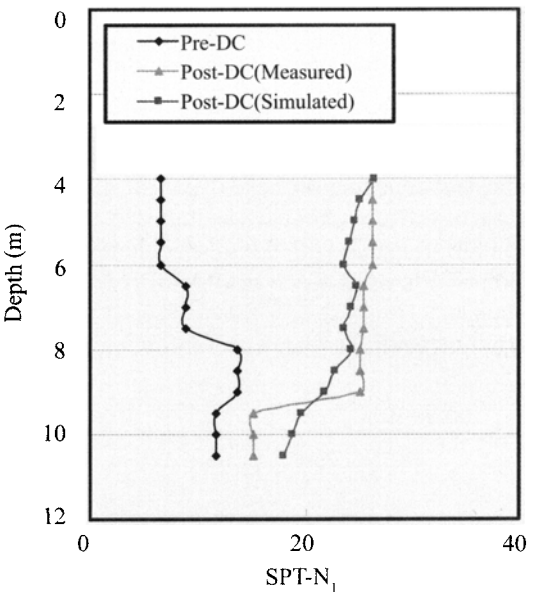

Fig. 12 Pre- and post-D.C. SPT blow counts (Steinaker dam modification project, Utah)

3.2.2 Parameters affecting densification

Following reasonable comparisons with case history data described above for both sand (without drains) and silty soils with wick drains, the above computational simulation model was used to assess the effect of the following parameters on densification by dynamic compaction in sands and silty sands: (i) hydraulic conductivity k and fines content F_C, (ii) impact grid pattern, (iii) impact print spacing, (iv) number of impacts, (v) time cycle between passes / impacts, (vi) wick drains spacing, and (vii) initial relative density. The results from this study are presented in Nashed (2004). Out of the parameters mentioned above, the following section is focusing on the effect of hydraulic conductivity and fines content on depth of influence. Numerical simulations were carried out on two silty soils with the same equivalent relative density of 40% but different hydraulic conductivities (a silty sand at k=10^{-7} m/s at fines content F_C of 25%; and a sandy silt at k=10^{-8} m/s at F_C=40%). The deposit was supplemented with wick drains of an equivalent diameter of 5 cm installed at a center-to-center spacing of 1.5 m in a square

pattern. The ground water table was assumed to be at 2 m depth, and the time cycle between subsequent impacts was selected as two minutes. The same impact grid pattern used for the Steinaker dam project (Fig. 13) was adopted. Three energy-delivery passes (primary, secondary, and tertiary) were made. Each grid point received a total of 12 impacts. The cumulative energy applied ranged from 1 to 3 MJ/m^2.

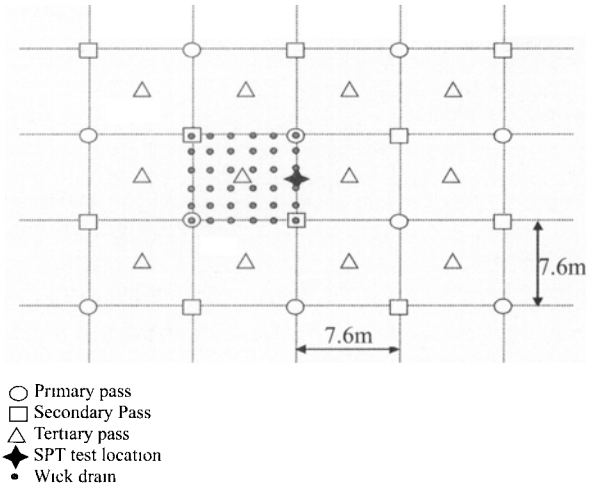

Fig. 13 Impact grid pattern - Steinaker dam

For comparison purposes, a second set of simulations was done for a sand deposit with k of 10^{-5} m/s at an initial relative density of 40%, without wick drains. A typical impact grid pattern for sand with 6.0 m spacing between the impact points was used. Each grid point received a total of 12 impacts.

The simulation results for depth of improvement d_{max} versus energy/impact for the silty soils with wick drains are shown in Fig.14(a), and for sand without wick drains are shown in Fig.14(b). Also shown in these figures is Eq.(1) for highly pervious sands (n=0.5), without wick drains. It is interesting to note the effects of fines and hydraulic conductivity on d_{max} in silty soils. A decrease in hydraulic conductivity reduces the effective depth of influence d_{max} (Nashed, 2004). When compared with Fig.14(b), the results indicate that, with the provision of wick drains, silty soils can be improved up to depths comparable for sands without wick drains.

Although further details of the study are not shown here, results indicate that D.C. is ineffective in silty soils with hydraulic conductivity less than 10^{-6} m/s, without wick drains. With wick drains, however, silty soils with hydraulic conductivities as low as 10^{-8} m/s could be densified using D.C. by pre-installing wick drains at a spacing of 1m to 1.5m.

The numerical simulation tool presented herein allows a designer or a contractor to study the effects of various site conditions and construction/design choices on the efficiency of D.C. process and arrive at an optimum design choice beyond what is currently possible with the use of Eq.1. Final guidelines for using D.C. to densify saturated silty soils supplemented with wick drains will be presented in Nashed (2004).

4 Conclusions

A semi-theoretical framework was developed to simulate ground response and analyze the densification process in saturated sands and non-plastic silty soils during vibro-stone column installation and dynamic compaction operations.

For vibro-stone column technique, the analysis includes two phenomena, (a) vibration-induced excess

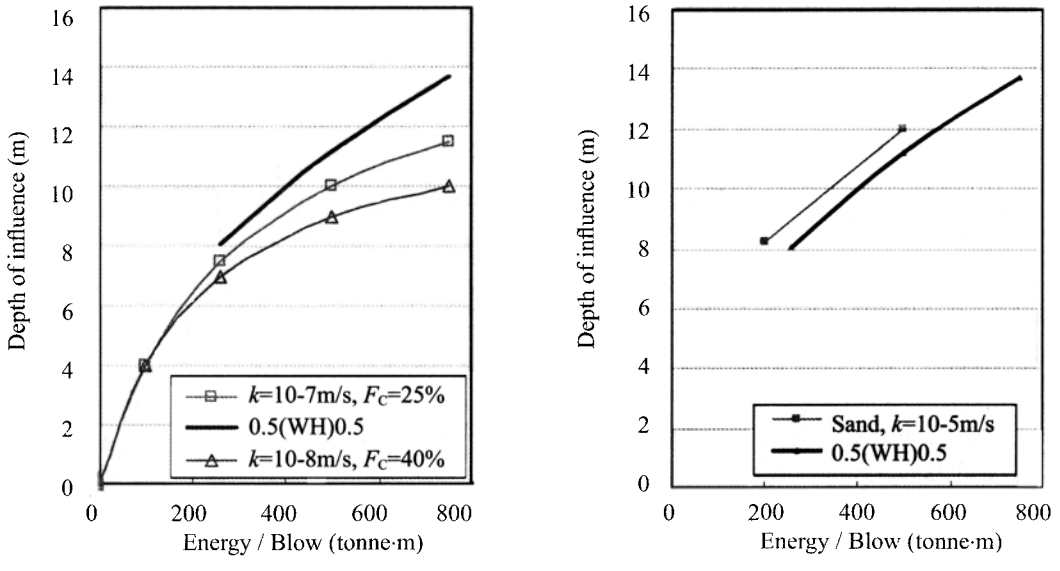

(a) Silty soil with wick drain (b) Sand without wick drain

Fig. 14 Effect of hydraulic conductivity and fines content on depth of influence

pore pressure development and concurrent dissipation and densification, and (b) cavity expansion-induced excess pore pressure development and concurrent dissipation and densification. Two factors have been identified important: (i) Area replacement ratio A_r, and (ii) hydraulic conductivity and silt content. For dynamic compaction, effects of site conditions, and the operational parameters of the technique were studied.

The results indicate that silty soils with hydraulic conductivities as low as 10^{-8} m/s could be densified using stone column at a close spacing of about 2 diameters or less with an area replacement ratio of about 20% or more supplemented with wick drains. Also for D.C. using wick drains in such low permeable soils improve the drainage rate and decreases consolidation time, making it possible to achieve depth of improvement as high as that is possible in sand deposits. Soils at hydraulic conductivities higher than about 10^{-6}m/s may be densified using either technique, without supplementary drainage systems.

The computational methodology presented herein is a powerful tool for design analyses of stone columns and dynamic compaction taking into account the site conditions and operational parameters for different deposits. The model is expected to advance the use of S.C. and D.C. in silty soils, and reduce the reliance on expensive field trials as a design tool. Ongoing further work focuses on developing design charts and design guidelines for both composite S.C. and composite D.C. techniques.

References

Andrews DCA (1998), "Liquefaction of Silty Soils: Susceptibility, Deformation, and Remediation," *Ph.D. Dissertation*, Dept. of Civil Eng., USC, CA.

Andrus RD and Chung RM (1995), "Ground Improvement Techniques for Liquefaction Remediation Near Existing Lifelines," *NISTIR Report # 5714*, Building and Fire Research Laboratory, National Institude of Standards and Technology, Gaithersburg, MD 20899.

Baez JI (1995), "A Design Model for the Reduction of Soil Liquefaction by Vibro-stone Columns," *Ph.D. Dissertation*, USC, Los Angeles, CA, pp. 207.

Chow YK, Yong DM, Yong KY and Lee S L (1992), "Dynamic Compaction Analysis," ASCE, *J. of Geotech. Engrg.*, **118**: 1141-1157.

Dise K, Stevens MG and Von Thun JL (1994), "Dynamic Compaction to Remediate Liquefiable Embankment Foundation Soils," *GSP No.45*, ASCE National Convention, Reston, VA, pp.1-25.

Dowding CH (1996), *Construction Vibrations*, Prentice Hall, Upper Saddle River, NJ.

FWHA (2001), "Stone Columns," *Ground Improvement Technical Summaries, II*, Federal Highway Administration, *Rep. No. FHWA-SA-98-086R.*

Luehring R, Snorteland N, Mejia L and Stevens M (2001), "Liquefaction Mitigation of a Silty Dam Foundation Using Vibro-stone Columns and Drainage Wicks: A Case History at Salmon Lake Dam," *Proc. 21st USSD annual meeting and lecture*, Denver, CO.

Lukas RG (1986), "Dynamic Compaction for Highway Construction, Vol. 1, Design and Construction Guidelines," Federal Highway Administration, *Rep. No. FHWA/RD86/133.*

Lukas RG (1995), "Dynamic Compaction", Federal Highway Administration, *Rep. No. FHWA-SA-95-037.*

Mayne PW (1985), "Ground Vibrations During Dynamic Compaction," In: Gazetas G, Selig ET, editors., *Vibration problems in geotechnical engineering*, ASCE, pp.247–265.

Meek JW and Wolf JP (1993), "Cone Models for Nearly Incompressible Soil," *Earthquake Engrg. and Struct. Dyn.*, **22**: 649-663.

Miller GF and Pursey H (1955), "On the Partition of Energy Between Elastic Waves in a Semi-infinite Soild," *Proc. Roy. Soc.*, A233, 55-69.

Mitchell JK, Baxter CDP and Munson TC (1995), "Performance of Improved Ground During Earthquakes," *Soil Improvement for Earthquake Hazard Mitigation, Proc., ASCE Convention, GSP 49*, Hryciw RD, edr., ASCE, San Diego, CA, pp.1-36.

Nashed R (2004), "Liquefaction Mitigation of Silty Soils Using Dynamic Compaction," *Ph.D. Dissertation*, University at Buffalo, Buffalo, NY, *In Preparation.*

Richart FE, Woods RD and Hall JR (1970), *Vibrations of Soils and Foundations*, Prentice Hall, Englewood Cliffs, NJ.

Seed HB, Martin PP and Lysmer J (1975), "The Generation and Dissipation of Pore Water Pressures During Soil Liquefaction," *Rep. No. UCB/EERC 75-26*, Earthq. Eng. Research Ctr., UC Berkeley, CA.

Shenthan T (2001), "Factors Affecting Liquefaction Mitigation in Silty Soils Using Stone Columns," *M S Thesis*, University at Buffalo, NY, pp. 220.

Shenthan T (2004), "Liquefaction Mitigation in Silty Soils Using Composite Stone Column," *Ph.D. Dissertation*, University at Buffalo, Buffalo, NY, In Preparation.

Shenthan T, Thevanayagam S and Martin GR (2004), "Ground Remediation for Silty Soils Using Composite Stone Columns - Contribution of Cavity Expansion to Densification," *MCEER Annual Report for Research Year 4, FHWA Contract # DTFH61-98-C-00094.*

Thevanayagam S, Martin GR, Shenthan T and Liang J (2001), "Post-liquefaction Pore Pressure Dissipation and Densification in Silty Soils," *Proc. 4th Int. Conf. on Recent Adv. in Geot. Earthq. Eng. and Soil Dyn.*, San Diego, CA, Paper 4.28.

Thevanayagam S and Martin GR (2001), "Liquefaction and Post-liquefaction Dissipation/densification Chara-

cteristics of Silty Soils," *MCEER Annual Report for Research Year 1, FHWA Contract #DTFH61-98-C-00094.*

Thevanayagam S, Kanagalingam T and Shenthan T (2002), "Contact Density – Confining Stress – Energy to Liquefaction," *Proc. 15th ASCE Eng. Mech. Conf.*, Columbia Univ., NY.

Thevanayagam S, Nashed R, Martin GR and Shenthan T (2004), "Ground Remediation for Silty Soils Using Composite Dynamic Compaction," *MCEER Annual Report for Research Year 4, FHWA Contract # DTFH61-98-C-00094.*

Tokimatsu K and Seed HB (1984), "Simplified Procedures for the Evaluation of Settlements in Sands Due to Earthquake Shaking," *EERC Report No. UCB/EERC-84/16*, UC Berkeley, CA.